HOMOGENIZATION OF TEMPERATURE-DEPENDENT SHORT FIBER REINFORCED POLYPROPYLEN AND EXPERIMENTAL INVESTIGATIONS OF LONG FIBER REINFORCED VINYLESTER

L. Kehrer[1], P. Pinter[2], T. Böhlke[3]

[1]Institute of Engineering Mechanics, Chair for Continuum Mechanics, Karlsruhe Institute of Technology (KIT), Kaiserstr. 10, Germany
Email: loredana.kehrer@kit.edu, Web Page: http://www.itm.kit.edu/english/cm
[2]Institute of Applied Materials, Karlsruhe Institute of Technology (KIT), Kaiserstr. 10, Germany
Email: pascal.pinter@kit.edu, Web Page: http://www.iam.kit.edu
[3]Institute of Engineering Mechanics, Chair for Continuum Mechanics, Karlsruhe Institute of Technology (KIT), Kaiserstr. 10, Germany
Email: thomas.boehlke@kit.edu, Web Page: http://www.itm.kit.edu/english/cm

Keywords: homogenization, short fiber reinforced composite, long fiber reinforced composite, μCT data, dynamic mechanical analysis

Abstract
In order to predict the elastic material properties of a short fiber reinforced composite, the self-consistent scheme and the interaction direct derivative method are used. Furthermore, thermoelastic effective material properties are calculated by the Hashin-Shtrikman two-step method using a reference stiffness that is variable, dependent on a scalar parameter. Within the homogenization methods, information on the microstructure obtained by μCT scans are considered. Using dynamic mechanical analysis (DMA), the material properties of long fiber reinforced polymers (LFRP) and short fiber reinforced polymers (SFRP) are investigated by tension tests under thermal load. The homogenized material properties of SFRP are compared with experimental results obtained by DMA.

1. Introduction

Lightweight materials based on fiber reinforced polymers are increasingly applied in different engineering applications due to their specific material properties. Especially in the automotive sector, there is a need for reinforced composite materials to gain resource-efficient constructions. Within an integrated engineering of reinforced polymer structures, the focus lies on a new class of lightweight materials. This new class of materials combines discontinuous and continuous fiber reinforced thermoset materials in order to achieve, e.g., a good formability, high stiffness and strength. To focus on discontinuous fiber reinforced polymers, short fiber reinforced polypropylen (PPGF30) and long fiber reinforced vinylester (VE-GF) are considered in this work. The material behavior of both, thermoset and thermoplastic material, is temperature-dependent and coupled to temperature history. The fabrication process by injection molding for PPGF30 and by sheet molding compound for VE-GF introduces a local fiber orientation distribution. By means of μCT scans, the microstructure of both, PPGF30 and VE-GF, is determined. This information on fiber length, fiber orientation and position can be used within a homogenization method to calculate effective material properties. There are many homogenization schemes for estimating the material response with various advantages and disadvantages. A commonly used method, the Mori-Tanaka homogenization method, has a simple structure. The method does, however, not consider inclusion in-

Excerpt from ISBN 978-3-00-053387-7

teraction or inclusion distribution. Based on a variational principle, Hashin and Shtrikman formulated the Hashin-Shtrikman bounds which were generalized by Willis for polycrystals and composites, containing unidirectional inclusions. The Hashin-Shtrikman bounds are given by an explicite expression. Moreover, the method considers inclusion interaction. Using the self-consistent scheme, various inclusion geometries and material properties can be considered additionally to the inclusion interaction. The generalized as well as the effective self-consistent scheme account for inclusion distribution in addition to the advantages mentioned. Hence, a main disadvantage of these methods is their implicite structure. Based on the effective self-consistent scheme, the interaction direct derivative is formulated explicitely, however, only for calculating elastic material properties. In the work at hand, the self-consistent scheme, the interaction direct derivative and the Hashin-Shtrikman two-step method are used. In Sec. 2, these homogenization methods are introduced. Information on the microstructure of the SFRP is given in Sec. 3.1 and in Sec. 4.1 for the LFRP, respectively. Experimental results for both materials are shown in Sec. 3.2 and in Sec. 4.2. Simulation results for the SFRP material are compared to experimental data in Sec. 5. Finally, a conclusion is given in Sec. 6.

Notation. In this work, a direct tensor notation is used. Scalars are denoted by lowercase letters, e.g. a, and Vectors by lowercase bold letters, e.g. $\boldsymbol{a}$. Second-order tensors and fourth-order tensors are indicated by $\boldsymbol{A}$ and $\mathbb{A}$, respectively. The scalar product and the dyadic product are formulated by $\boldsymbol{A} \cdot \boldsymbol{B}$ and $\boldsymbol{A} \otimes \boldsymbol{B}$. The composition of two tensors of the same order is given by $\boldsymbol{A}\boldsymbol{B}$ and $\mathbb{A}\mathbb{B}$, respectively. A linear mapping is denoted by $\boldsymbol{A} = \mathbb{C}[\boldsymbol{B}]$. By the means of $\mathbb{I}^{\mathrm{S}}$ the identity on symmetric tensors of second order is given. The brackets $\langle\cdot\rangle$ are defined as ensemble average that corresponds to volume average in the infinite volume limit for ergodic media .

2. Homogenization methods

2.1. Self-consistent method

The composite material consists of n glass fibers embedded in a polymer matrix. It is assumed that both, fiber and matrix material, provide isotropic and piecewise constant material properties. The self-consistent (SC) method was originally developed by [1] and [2]. Regarding the SC method, a single fiber is embedded in an infinite homogeneous matrix, providing effective, yet unknown, material properties. In order to account for thermal strains, the eigenstrain concept proposed by [3] leads to the effective material stiffness $\bar{\mathbb{C}}^{\mathrm{SC}}$ by the SC method

$$\bar{\mathbb{C}}^{\mathrm{SC}} = \mathbb{C}_{\mathrm{M}} + \sum_{\alpha=1}^{\mathrm{n}} c_\alpha (\mathbb{C}_\alpha - \mathbb{C}_{\mathrm{M}}) \mathbb{A}_\alpha, \qquad \mathbb{A}_\alpha = \left(\mathbb{I}^{\mathrm{S}} + \mathbb{P}_\alpha (\mathbb{C}_\alpha - \bar{\mathbb{C}}^{\mathrm{SC}})\right)^{-1}, \qquad \mathbb{P}_\alpha = \mathbb{P}_\alpha(\bar{\mathbb{C}}^{\mathrm{SC}}, \boldsymbol{Z}_\alpha). \tag{1}$$

The matrix material is denoted by a subscripted M, and index $\alpha = 1, \ldots, n$ depicts the modeled fibers. Thus, $\mathbb{C}_{\mathrm{M}}$ indicates the stiffness of matrix material and $\mathbb{C}_\alpha$ the stiffness of a fiber α, respectively. Furthermore, the fiber volume fraction is given by c_α and $c_{\mathrm{M}} = 1 - \sum_{\alpha=1}^{n} c_\alpha$ holds. Besides, the strain localization tensor is denoted by $\mathbb{A}$ and Hill's polarization tensor by $\mathbb{P}$. The geometry matrix $\boldsymbol{Z}$ contains the ratio of the half axes of the fiber geometry, modeled as ellipsoids.

2.2. Interaction direct derivative method

The interaction direct derivative (IDD) estimate is proposed by [4] and based on the three-phase model. The three-phase model contains an inclusion that is embedded in a finite matrix material. Both, the inclusion and the matrix, called matrix-inclusion cell, are embedded in an infinite effective medium, cf.,

Excerpt from ISBN 978-3-00-053387-7

e.g., [5]. According to [4], the effective stiffness $\bar{\mathbb{C}}^{\mathrm{IDD}}$ is calculated by

$$\bar{\mathbb{C}}^{\mathrm{IDD}} = \mathbb{C}_{\mathrm{M}} + \left(\mathbb{I}^{\mathrm{S}} - \sum_{\alpha=1}^{n} c_\alpha \delta\mathbb{C}_\alpha \mathbb{M}_\alpha \mathbb{P}_\alpha^D \right)^{-1} \sum_{\beta=1}^{n} c_\beta \delta\mathbb{C}_\beta \mathbb{M}_\beta, \;\; \delta\mathbb{C}_\alpha = \mathbb{C}_\alpha - \mathbb{C}_{\mathrm{M}}, \; \mathbb{M}_\alpha = \left(\mathbb{I}^{\mathrm{S}} + \mathbb{P}_\alpha \delta\mathbb{C}_\alpha \right)^{-1}. \quad (2)$$

For distributed inclusions, Hill's polarization tensor is given for the matrix-inclusion cell by $\mathbb{P}_\alpha^{\mathrm{D}} = \mathbb{P}(\mathbb{C}_{\mathrm{M}}, \boldsymbol{Z}_\alpha^{\mathrm{D}})$. In the following, an identical shape of matrix-inclusion cell and inclusion, $\boldsymbol{Z}_\alpha^{\mathrm{D}} = \boldsymbol{Z}_\alpha$, is assumed.

2.3. Hashin-Shtrikman two-step method

In [3], the generalized Hashin-Shtrikman variational approach for second order homogenization is extended in order to account for eigenstrains. Using this formulation, a two-step method is derived. In the first step, the microstructure is divided into domains, containing a fiber of certain orientation, embedded into matrix material. For each domain α, the effective thermal and mechanical properties are determined using the upper and lower Hashin-Shtrikman bounds. The effective stiffness and the effective thermal expansion are calculated for the special case of unidirectional aligned fibers in each domain by

$$\bar{\mathbb{C}}_\alpha^{\mathrm{UD}+} = \mathbb{C}_\alpha + c_{\mathrm{M}}(\mathbb{C}_{\mathrm{M}} - \mathbb{C}_\alpha)\Big(\mathbb{I}^{\mathrm{S}} + c_\alpha \mathbb{P}_\alpha^{\mathrm{UD}} (\mathbb{C}_{\mathrm{M}} - \mathbb{C}_\alpha) \Big)^{-1}, \quad (3)$$

$$\bar{\mathbb{C}}_\alpha^{\mathrm{UD}-} = \mathbb{C}_{\mathrm{M}} + c_\alpha(\mathbb{C}_\alpha - \mathbb{C}_{\mathrm{M}})\Big(\mathbb{I}^{\mathrm{S}} + c_{\mathrm{M}} \mathbb{P}_\alpha^{\mathrm{UD}} (\mathbb{C}_\alpha - \mathbb{C}_{\mathrm{M}}) \Big)^{-1}, \quad (4)$$

$$\bar{\boldsymbol{\alpha}}^{\mathrm{UD}+} = \left(\bar{\mathbb{C}}_\alpha^{\mathrm{UD}+} \right)^{-1} \Big(\mathbb{C}_\alpha[\boldsymbol{\alpha}_\alpha] + c_{\mathrm{M}} \Big(\mathbb{I}^{\mathrm{S}} + c_\alpha \mathbb{P}_\alpha^{\mathrm{UD}} (\mathbb{C}_{\mathrm{M}} - \mathbb{C}_\alpha) \Big)^{-\mathrm{T_H}} \Big(\mathbb{C}_{\mathrm{M}}[\boldsymbol{\alpha}_{\mathrm{M}}] - \mathbb{C}_\alpha[\boldsymbol{\alpha}_\alpha] \Big) \Big), \quad (5)$$

$$\bar{\boldsymbol{\alpha}}^{\mathrm{UD}-} = \left(\bar{\mathbb{C}}_\alpha^{\mathrm{UD}-} \right)^{-1} \Big(\mathbb{C}_{\mathrm{M}}[\boldsymbol{\alpha}_{\mathrm{M}}] + c_\alpha \Big(\mathbb{I}^{\mathrm{S}} + c_{\mathrm{M}} \mathbb{P}_\alpha^{\mathrm{UD}} (\mathbb{C}_\alpha - \mathbb{C}_{\mathrm{M}}) \Big)^{-\mathrm{T_H}} \Big(\mathbb{C}_\alpha[\boldsymbol{\alpha}_\alpha] - \mathbb{C}_{\mathrm{M}}[\boldsymbol{\alpha}_{\mathrm{M}}] \Big) \Big). \quad (6)$$

In this context, Hill's polarization tensor is given explicitly, cf., e.g, [3]. In the second step, the total effective material properties are determined by using the Hashin-Shtrikman bounding method

$$\bar{\mathbb{C}}^{\mathrm{HS}\pm} = \sum_{\alpha=1}^{n} \frac{c_\alpha}{c_{\mathrm{F}}} \bar{\mathbb{C}}_\alpha^{\mathrm{UD}\pm} \mathbb{A}_\alpha^{\mathrm{HS}} = \sum_{\alpha=1}^{n} \bar{\mathbb{C}}_\alpha^{\mathrm{UD}\pm} \mathbb{M}_\alpha \langle \mathbb{M} \rangle^{-1}, \quad (7)$$

$$\bar{\boldsymbol{\alpha}}^{\mathrm{HS}\pm} = \sum_{\alpha=1}^{n} \frac{c_\alpha}{c_{\mathrm{F}}} \left(\bar{\mathbb{C}}^{\mathrm{HS}\pm} \right)^{-1} \left(\langle \mathbb{M} \rangle^{-1} \right)^{\mathrm{T_H}} \mathbb{M}_\alpha^{\mathrm{T_H}} \bar{\mathbb{C}}_\alpha^{\mathrm{UD}\pm} [\bar{\boldsymbol{\alpha}}_\alpha^{\mathrm{UD}\pm}], \quad (8)$$

$$\mathbb{M}_\alpha = \left(\mathbb{I}^{\mathrm{S}} + \mathbb{P}_0 (\bar{\mathbb{C}}_\alpha^{\mathrm{UD}\pm} - \mathbb{C}_0) \right)^{-1}, \quad \langle \mathbb{M} \rangle = \sum_{\alpha=1}^{n} \frac{c_\alpha}{c_{\mathrm{F}}} \mathbb{M}_\alpha, \quad (9)$$

with c_{F} denoting the total fiber volume fraction. The overall material properties, calculated by Eq. (7) and (8), are evaluated by assuming an isotropic two-point correlation function for each domain and contain the reference stiffness $\mathbb{C}_0$. In the work at hand, the reference stiffness depends on the parameter a, such that

$$\mathbb{C}_0 = (1 - a)\mathbb{C}_{\mathrm{M}} + a\mathbb{C}_{\mathrm{F}} \quad (10)$$

holds. The parameter a is selected in the range between 0 and 1 leading to $\mathbb{C}_0 = \mathbb{C}_{\mathrm{M}}$ for $a = 0$ and $\mathbb{C}_0 = \mathbb{C}_{\mathrm{F}}$ for $a = 1$, respectively.

3. Short fiber reinforced polymers

3.1. Microstructure

The SFRP material consists of polypropylen (PP) as matrix material, reinforced with 30 wt.% of short glass fibers (PPGF30). Plates of reinforced and pure PP are manufactured by injection molding. Samples

Excerpt from ISBN 978-3-00-053387-7

are taken from the plates at 0°, 45° and 90° relative to the direction of injection. Based on µCT scans, the microstructure of the composite material is determined, resulting in approximately 7000 fibers with variation on length, position and orientation of the fibers in the sample. A reconstruction of the fibers is depicted in Fig. 1(a). Using a continuous representation of the stereographic projection of the µCT data, Fig. 1(b) shows that most of the fibers are orientated in direction of injection molding. A detailed evaluation of the microstructure and information on the material configuration are given in [6].

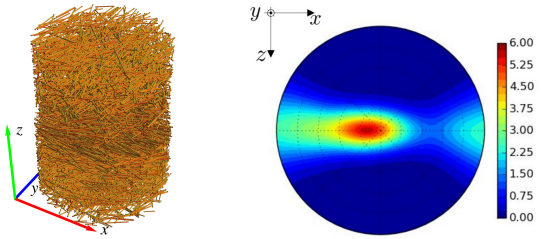

(a) (b)

Figure 1. (a) Microstructure and (b) continuous pole figure of short fiber reinforced polypropylen based on µCT data

3.2. Experimental investigations

By means of dynamic mechanical tension tests under thermal load, using the DMA system GABO Eplexor® 500N, the temperature-dependent viscoelastic material properties of PP and PPGF30 are determined. The tests are performed using a load cell with a capacity of 500 N. Moreover, the thermal load increases with a heating rate of 1 K/min from −50°C to 120°C. The geometry of the samples is defined by 80 mm × 12.3 mm × 2.3 mm. In Fig. 2 the results are depicted. As anticipated, the storage modulus exhibits a temperature-dependent behavior. The composite material reveals anisotropic material behavior, depicted by a higher storage modulus for 0° direction compared to 45° and 90° direction. Increasing viscoelastic material behavior of both, PP and PPGF30, is observed for temperatures higher than −10°C and a loss factor $\tan\delta \geq 0.02$.

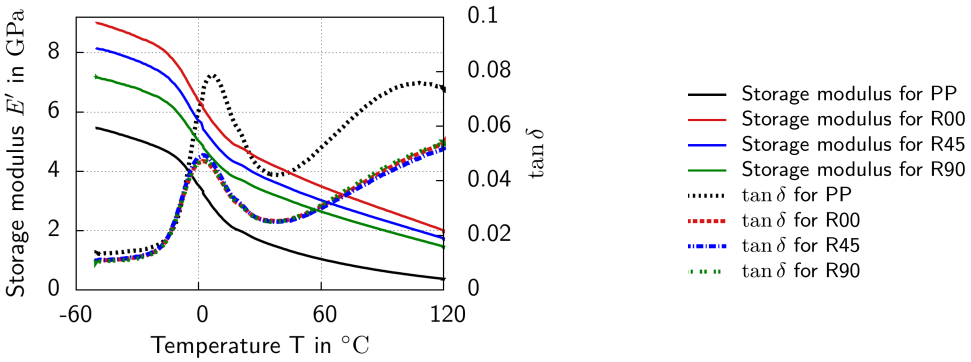

Figure 2. DMA tension test under thermal load for pure PP and PPGF30 at 0° (R00), 45° (R45) and 90° (R90) relative to direction of injection

Excerpt from ISBN 978-3-00-053387-7

4. Long fiber reinforced polymers

4.1. Microstructure

The second class of materials is based on vinylester resin reinforced with chopped, long glass fibers with a fiber volume fraction of 23 %. Specimens of pure and reinforced vinylester are manufactured by sheet molding compound. In this work, filling the mold with resin at 33 % leads to flow during the press process. By this fabrication process, a local fiber orientation distribution is introduced. Fig. 3 depicts the microstructure based on a µCT scan. The present CT scan was carried out on a YXLON precision computed tomography system containing an open X-ray reflection tube with tungsten target, and a 2048 × 2048 pixel flat panel detector with a pixel pitch of 200 µm from Perkin Elmer. The image has a resolution of 5.3 µm/voxel and was acquired with an acceleration voltage of 80 kV and a target current of 0.1 mA.

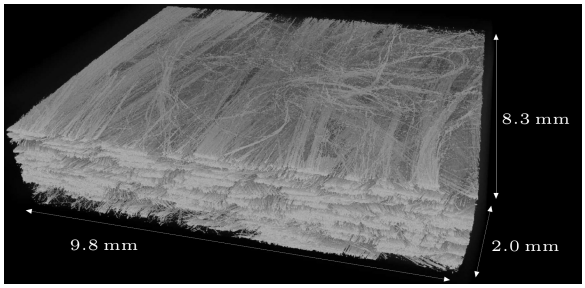

Figure 3. Microstructure of discontinuous long fiber reinforced vinylester based on µCT scan

4.2. Experimental investigations

Analogous to the experimental investigations for SFRP using DMA, see Sec. 3.2, the storage modulus for the LFRP is determined by thermomechanical tension mode. During the dynamic mechanical tension, the temperature load varies between −50°C and 150°C with a heating rate of 1 K/min. In Fig. 4, the storage modulus E' and $\tan\delta$ depicted over the temperature is shown. In contrast to the SFRP, the LFRP material shows a higher anisotropic material behavior. This is indicated by a higher distance between the storage modulus for the sample loaded longitudinal to fiber direction and the storage modulus for the sample loaded transverse to fiber direction, cf. 0° and 90° direction in Fig. 4. Due to the fact, that the temperature range is below the glass transition temperature, no peak of $\tan\delta$ and lower changes of E' have been observed. Hence, with higher temperature $\tan\delta$ increases, especially from $T = 100$°C on.

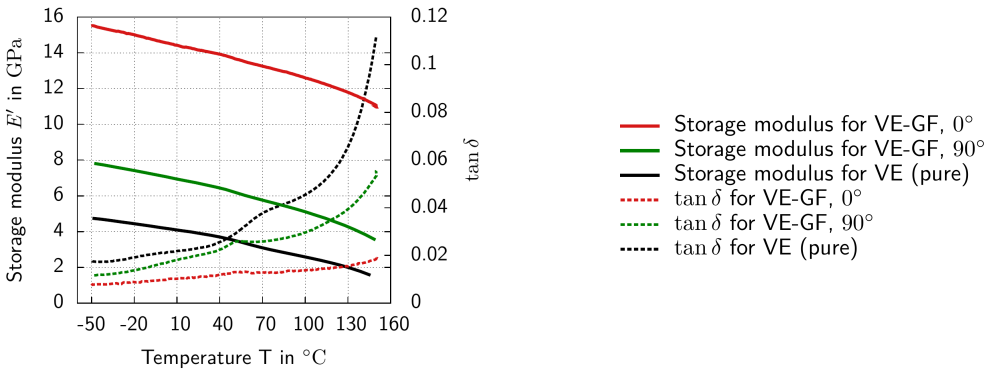

Figure 4. DMA tension test under thermal load for pure and long glass fiber reinforced vinylester

Excerpt from ISBN 978-3-00-053387-7

5. Comparison of experimental and simulation results

5.1. Comparison of homogenization methods for SFRP

By means of the homogenization methods introduced in Sec. 2, the effective material properties are calculated, accounting for fiber orientation, length and diameter which are obtained by µCT scans. In order to compare simulation results for the different homogenization methods with both each other and experimental results, the orientation-dependent Young's modulus $E(\boldsymbol{d})$, given by

$$\frac{1}{E(\boldsymbol{d})} = \boldsymbol{d} \otimes \boldsymbol{d} \cdot \mathbb{C}^{-1}[\boldsymbol{d} \otimes \boldsymbol{d}], \tag{11}$$

is depicted in Fig. 5. The upper and lower Hashin-Shtrikman bounds for the two-step method compared to results by the SC and IDD method are shown in Fig. 5(a) to (c), and in Fig. 5(d) to (f), respectively. In

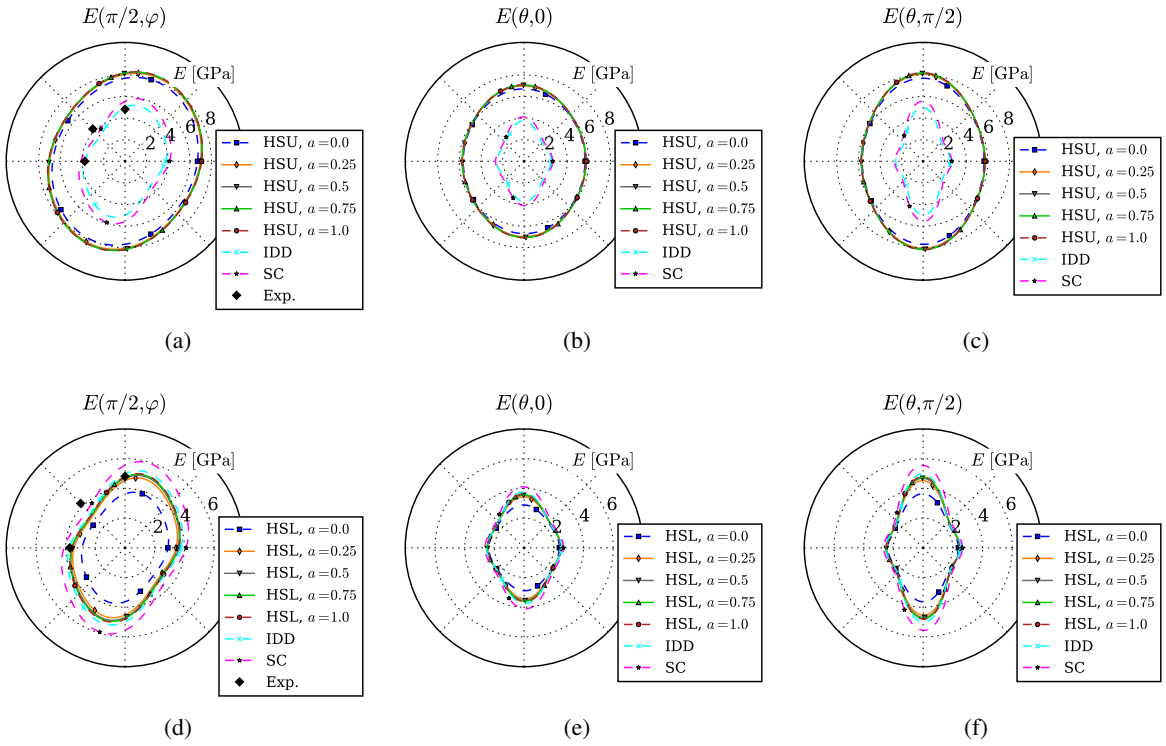

Figure 5. Contour plot for orientation-dependent Young's modulus obtained by different homogenization schemes

the first row, HSU shows for any choices of parameter a a higher deviation from both experimental results and simulation results by SC and IDD. In the second row, three main results are observed. Compared to the simulation results obtained by SC and IDD, HSL is more compliant. The stiffest results are obtained by the SC scheme. Secondly, the parameter a influences the numerical results for the two-step method. As Fig. 5(d) shows, the SC method overestimates the experimental results for 0° and 90° specimens. In this context, results by IDD and HSL for $a \geq 0.25$ exhibit the smallest deviations. In addition to the overestimation, the SC method provides, moreover, disadvantages concerning the calculation time due to its implicit structure. With regard to the IDD method, the literature does not provide an extension using eigenstrains, in order to account for thermoelastic material behavior. Thus, the HSL is investigated in the following section for further analysis.

Excerpt from ISBN 978-3-00-053387-7

5.2. Comparison of various a for $\mathbb{C}_0$ for different temperature loads

Fig. 6 depicts the contour plot in the x-y plane for Young's modulus, calculated by Eqs. (4) and (7), and for thermal expansion, calculated by Eqs. (6) and (8). Regarding Sec. 3.1, the main fiber direction is in y-direction which is reflected by the effective Young's modulus in Fig. 6(a). The thermal expansion of matrix material is higher compared to the fiber material. Thus, Fig. 6(b) shows a higher effective thermal expansion in direction transverse to fiber direction and smaller values longitudinal to fiber direction, respectively.

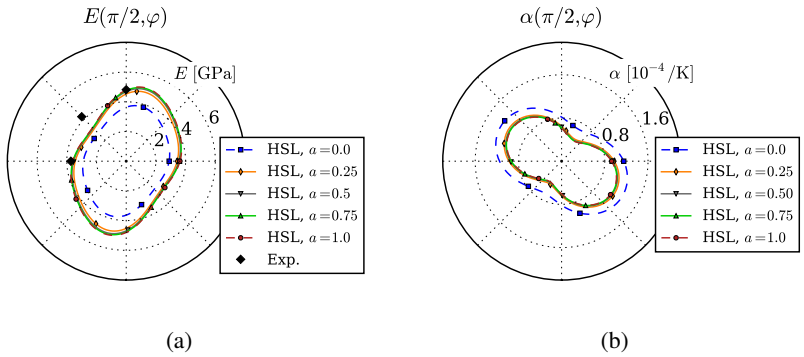

(a) (b)

Figure 6. Contour plot for Young's modulus and thermal expansion for different values for a

Considering that the effective material properties are evaluated for all three orientations of specimen, the choice of $a = 0.75$ shows the smallest deviation from experimental results and is chosen for further investigations. Due to the thermoelastic material behavior, the effective stiffness is calculated for the thermal load from -50°C to 120°C. Fig. 7 depicts the deviation from experimental results, evaluated in the three directions 0°, 45° and 90°. The calculations exhibit, for the entire temperature load, a deviation of maximum 5 % for the 0° specimen and about 10 % for the 45° specimen. A higher deviation, of about 15 %, is given for the 90° specimen. This indicates that the material behavior transverse to fiber direction is influenced by a matrix material which behaves viscoelastic for increasing temperatures. Since the viscoelastic material behavior is not considered yet, the relative error between experimental and simulation results increases. Fig. 7(b) shows the deviation at $T = 20°$.

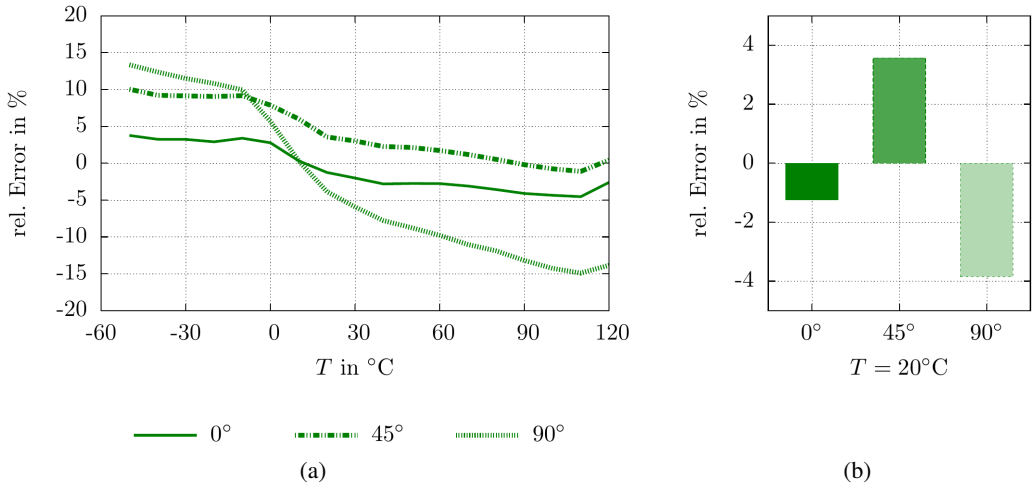

(a) (b)

Figure 7. Comparison of deviation for different orientation of specimen for $a = 0.75$

Excerpt from ISBN 978-3-00-053387-7

6. Summary and conclusion

In the work at hand, two classes of fiber reinforced polymers are considered: short glass fiber reinforced polypropylen (PPGF30) and long glass fiber reinforced vinylester (VE-GF). Preliminary investigations are performed by means of μCT scans in order to get information on the microstructure. Commonly known homogenization methods and an enhanced Hashin-Shtrikman two-step method are used to predict material behavior of the polymer material. The results of this methods are compared to experimental results for PPGF30. This comparison shows that the SC method overestimates the experimental results, whereas the results by IDD and HSL estimates are closer to the experimental data. For HSL, the effective Young's modulus and thermal expansion coefficient are calculated for a reference stiffness, dependent on different values for parameter a. Taking the smallest deviation of simulation results from experimental data into account, leads to the choice of $a = 0.75$. For a material behavior which is dominated by fiber material, the deviation is smaller than 10 %. The 90° oriented sample indicates that viscoelastic material behavior of matrix material has to be considered. Thus, the Hashin-Shtrikman two-step method has to be extended for further investigations. In order to apply the developed homogenization method on the long fiber reinforced vinylester, the long fibers can be modeled for a first approximation by shorter, straight segments. Calculation results can then be compared to both, experimental results and simulation results obtained by GeoDict®.

Acknowledgments

The research documented in this manuscript has been funded by the German Research Foundation (DFG) within the International Research Training Group "Integrated engineering of continuous-discontinuous long fiber reinforced polymer structures"(GRK 2078). The support by the German Research Foundation (DFG) is gratefully acknowledged. Special thanks go to Barthel Brylka for supporting the measurements with the DMA.

References

[1] A. V. Hershey. The elasticity of an isotropic aggregate of anisotropic cubic crystals. *Journal of Applied Mechanics-Transactions of the ASME*, 21(3):236–240, 1954.

[2] E. Kröner. Berechnung der elastischen Konstanten des Vielkristalls aus den Konstanten des Einkristalls. *Zeitschrift für Physik*, 151(4):504–518, 1958.

[3] J. R. Willis. Variational and related methods for the overall properties of composites. *Advances in Applied Mechanics*, 21, 1981.

[4] Q.-S. Zheng and D.-X. Du. An explicit and universally applicable estimate for the effective properties of multiphase composites which accounts for inclusion distribution. *Journal of the Mechanics and Physics of Solids*, 49(11):2765–2788, 2001.

[5] R. M. Christensen and K. H. Lo. Solutions for effective shear properties in three phase sphere and cylinder models. *Journal of the Mechanics and Physics of Solids*, 27(4):315–330, 1979.

[6] V. Müller, B. Brylka, F. Dillenberger, R. Glöckner, S. Kolling, and T. Böhlke. Homogenization of elastic properties of short-fiber reinforced composites based on measured microstructure data. *Journal of Composite Materials*, 0021998315574314, 2015.

Excerpt from ISBN 978-3-00-053387-7